J/ψ Production versus Centrality, Transverse Momentum, and Rapidity in Au + Au Collisions at $\sqrt{s_{NN}} = 200$ GeV

A. Adare,[8] S. Afanasiev,[22] C. Aidala,[9] N. N. Ajitanand,[49] Y. Akiba,[43,44] H. Al-Bataineh,[38] J. Alexander,[49] A. Al-Jamel,[38] K. Aoki,[28,43] L. Aphecetche,[51] R. Armendariz,[38] S. H. Aronson,[3] J. Asai,[44] E. T. Atomssa,[29] R. Averbeck,[50] T. C. Awes,[39] B. Azmoun,[3] V. Babintsev,[18] G. Baksay,[14] L. Baksay,[14] A. Baldisseri,[11] K. N. Barish,[4] P. D. Barnes,[31] B. Bassalleck,[37] S. Bathe,[4] S. Batsouli,[9,39] V. Baublis,[42] F. Bauer,[4] A. Bazilevsky,[3] S. Belikov,[3,21] R. Bennett,[50] Y. Berdnikov,[46] A. A. Bickley,[8] M. T. Bjorndal,[9] J. G. Boissevain,[31] H. Borel,[11] K. Boyle,[50] M. L. Brooks,[31] D. S. Brown,[38] D. Bucher,[34] H. Buesching,[3] V. Bumazhnov,[18] G. Bunce,[3,44] J. M. Burward-Hoy,[31] S. Butsyk,[31,50] S. Campbell,[50] J.-S. Chai,[23] B. S. Chang,[58] J.-L. Charvet,[11] S. Chernichenko,[18] J. Chiba,[24] C. Y. Chi,[9] M. Chiu,[9,19] I. J. Choi,[58] T. Chujo,[55] P. Chung,[49] A. Churyn,[18] V. Cianciolo,[39] C. R. Cleven,[16] Y. Cobigo,[11] B. A. Cole,[9] M. P. Comets,[40] P. Constantin,[21,31] M. Csanád,[13] T. Csörgő,[25] T. Dahms,[50] K. Das,[15] G. David,[3] M. B. Deaton,[1] K. Dehmelt,[14] H. Delagrange,[51] A. Denisov,[18] D. d'Enterria,[9] A. Deshpande,[44,50] E. J. Desmond,[3] O. Dietzsch,[47] A. Dion,[50] M. Donadelli,[47] J. L. Drachenberg,[1] O. Drapier,[29] A. Drees,[50] A. K. Dubey,[57] A. Durum,[18] V. Dzhordzhadze,[4,52] Y. V. Efremenko,[39] J. Egdemir,[50] F. Ellinghaus,[8] W. S. Emam,[4] A. Enokizono,[17,30] H. En'yo,[43,44] B. Espagnon,[40] S. Esumi,[54] K. O. Eyser,[4] D. E. Fields,[37,44] M. Finger,[5,22] F. Fleuret,[29] S. L. Fokin,[27] B. Forestier,[32] Z. Fraenkel,[57] J. E. Frantz,[9,50] A. Franz,[3] A. D. Frawley,[15] K. Fujiwara,[43] Y. Fukao,[28,43] S.-Y. Fung,[4] T. Fusayasu,[36] S. Gadrat,[32] I. Garishvili,[52] F. Gastineau,[51] M. Germain,[51] A. Glenn,[8,52] H. Gong,[50] M. Gonin,[29] J. Gosset,[11] Y. Goto,[43,44] R. Granier de Cassagnac,[29] N. Grau,[21] S. V. Greene,[55] M. Grosse Perdekamp,[19,44] T. Gunji,[7] H.-Å. Gustafsson,[33] T. Hachiya,[17,43] A. Hadj Henni,[51] C. Haegemann,[37] J. S. Haggerty,[3] M. N. Hagiwara,[1] H. Hamagaki,[7] R. Han,[41] H. Harada,[17] E. P. Hartouni,[30] K. Haruna,[17] M. Harvey,[3] E. Haslum,[33] K. Hasuko,[43] R. Hayano,[7] M. Heffner,[30] T. K. Hemmick,[50] T. Hester,[4] J. M. Heuser,[43] X. He,[16] H. Hiejima,[19] J. C. Hill,[21] R. Hobbs,[37] M. Hohlmann,[14] M. Holmes,[55] W. Holzmann,[49] K. Homma,[17] B. Hong,[26] T. Horaguchi,[43,53] D. Hornback,[52] M. G. Hur,[23] T. Ichihara,[43,44] K. Imai,[28,43] M. Inaba,[54] Y. Inoue,[45,43] D. Isenhower,[1] L. Isenhower,[1] M. Ishihara,[43] T. Isobe,[7] M. Issah,[49] A. Isupov,[22] B. V. Jacak,[50] J. Jia,[9] J. Jin,[9] O. Jinnouchi,[44] B. M. Johnson,[3] K. S. Joo,[35] D. Jouan,[40] F. Kajihara,[7,43] S. Kametani,[7,56] N. Kamihara,[43,53] J. Kamin,[50] M. Kaneta,[44] J. H. Kang,[58] H. Kanou,[43,53] T. Kawagishi,[54] D. Kawall,[44] A. V. Kazantsev,[27] S. Kelly,[8] A. Khanzadeev,[42] J. Kikuchi,[56] D. H. Kim,[35] D. J. Kim,[58] E. Kim,[48] Y.-S. Kim,[23] E. Kinney,[8] A. Kiss,[13] E. Kistenev,[3] A. Kiyomichi,[43] J. Klay,[30] C. Klein-Boesing,[34] L. Kochenda,[42] V. Kochetkov,[18] B. Komkov,[42] M. Konno,[54] D. Kotchetkov,[4] A. Kozlov,[57] A. Král,[10] A. Kravitz,[9] P. J. Kroon,[3] J. Kubart,[5,20] G. J. Kunde,[31] N. Kurihara,[7] K. Kurita,[45,43] M. J. Kweon,[26] Y. Kwon,[52,58] G. S. Kyle,[38] R. Lacey,[49] Y.-S. Lai,[9] J. G. Lajoie,[21] A. Lebedev,[21] Y. Le Bornec,[40] S. Leckey,[50] D. M. Lee,[31] M. K. Lee,[58] T. Lee,[48] M. J. Leitch,[31] M. A. L. Leite,[47] B. Lenzi,[47] H. Lim,[48] T. Liška,[10] A. Litvinenko,[22] M. X. Liu,[31] X. Li,[6] X. H. Li,[4] B. Love,[55] D. Lynch,[3] C. F. Maguire,[55] Y. I. Makdisi,[3] A. Malakhov,[22] M. D. Malik,[37] V. I. Manko,[27] Y. Mao,[41,43] L. Mašek,[5,20] H. Masui,[54] F. Matathias,[9,50] M. C. McCain,[19] M. McCumber,[50] P. L. McGaughey,[31] Y. Miake,[54] P. Mikeš,[5,20] K. Miki,[54] T. E. Miller,[55] A. Milov,[50] S. Mioduszewski,[3] G. C. Mishra,[16] M. Mishra,[2] J. T. Mitchell,[3] M. Mitrovski,[49] A. Morreale,[4] D. P. Morrison,[3] J. M. Moss,[31] T. V. Moukhanova,[27] D. Mukhopadhyay,[55] J. Murata,[45,43] S. Nagamiya,[24] Y. Nagata,[54] J. L. Nagle,[8] M. Naglis,[57] I. Nakagawa,[43,44] Y. Nakamiya,[17] T. Nakamura,[17] K. Nakano,[43,53] J. Newby,[30] M. Nguyen,[50] B. E. Norman,[31] A. S. Nyanin,[27] J. Nystrand,[33] E. O'Brien,[3] S. X. Oda,[7] C. A. Ogilvie,[21] H. Ohnishi,[43] I. D. Ojha,[55] H. Okada,[28,43] K. Okada,[44] M. Oka,[54] O. O. Omiwade,[1] A. Oskarsson,[33] I. Otterlund,[33] M. Ouchida,[17] K. Ozawa,[7] R. Pak,[3] D. Pal,[55] A. P. T. Palounek,[31] V. Pantuev,[50] V. Papavassiliou,[38] J. Park,[48] W. J. Park,[26] S. F. Pate,[38] H. Pei,[21] J.-C. Peng,[19] H. Pereira,[11] V. Peresedov,[22] D. Yu. Peressounko,[27] C. Pinkenburg,[3] R. P. Pisani,[3] M. L. Purschke,[3] A. K. Purwar,[31,50] H. Qu,[16] J. Rak,[21,37] A. Rakotozafindrabe,[29] I. Ravinovich,[57] K. F. Read,[39,52] S. Rembeczki,[14] M. Reuter,[50] K. Reygers,[34] V. Riabov,[42] Y. Riabov,[42] G. Roche,[32] A. Romana,[29,*] M. Rosati,[21] S. S. E. Rosendahl,[33] P. Rosnet,[32] P. Rukoyatkin,[22] V. L. Rykov,[43] S. S. Ryu,[58] B. Sahlmueller,[34] N. Saito,[28,43,44] T. Sakaguchi,[3,7,56] S. Sakai,[54] H. Sakata,[17] V. Samsonov,[42] H. D. Sato,[28,43] S. Sato,[3,24,54] S. Sawada,[24] J. Seele,[8] R. Seidl,[19] V. Semenov,[18] R. Seto,[4] D. Sharma,[57] T. K. Shea,[3] I. Shein,[18] A. Shevel,[42,49] T.-A. Shibata,[43,53] K. Shigaki,[17] M. Shimomura,[54] T. Shohjoh,[54] K. Shoji,[28,43] A. Sickles,[50] C. L. Silva,[47] D. Silvermyr,[39] C. Silvestre,[11] K. S. Sim,[26] C. P. Singh,[2] V. Singh,[2] S. Skutnik,[21] M. Slunečka,[5,22] W. C. Smith,[1] A. Soldatov,[18] R. A. Soltz,[30] W. E. Sondheim,[31] S. P. Sorensen,[52] I. V. Sourikova,[3] F. Staley,[11] P. W. Stankus,[39] E. Stenlund,[33] M. Stepanov,[38] A. Ster,[25] S. P. Stoll,[3] T. Sugitate,[17] C. Suire,[40] J. P. Sullivan,[31] J. Sziklai,[25] T. Tabaru,[44] S. Takagi,[54] E. M. Takagui,[47] A. Taketani,[43,44] K. H. Tanaka,[24] Y. Tanaka,[36] K. Tanida,[43,44] M. J. Tannenbaum,[3] A. Taranenko,[49] P. Tarján,[12] T. L. Thomas,[37] M. Togawa,[28,43] A. Toia,[50] J. Tojo,[43] L. Tomášek,[20]

H. Torii,[43] R. S. Towell,[1] V-N. Tram,[29] I. Tserruya,[57] Y. Tsuchimoto,[17,43] S. K. Tuli,[2] H. Tydesjö,[33] N. Tyurin,[18] C. Vale,[21] H. Valle,[55] H. W. van Hecke,[31] J. Velkovska,[55] R. Vertesi,[12] A. A. Vinogradov,[27] M. Virius,[10] V. Vrba,[20] E. Vznuzdaev,[42] M. Wagner,[28,43] D. Walker,[50] X. R. Wang,[38] Y. Watanabe,[43,44] J. Wessels,[34] S. N. White,[3] N. Willis,[40] D. Winter,[9] C. L. Woody,[3] M. Wysocki,[8] W. Xie,[4,44] Y. Yamaguchi,[56] A. Yanovich,[18] Z. Yasin,[4] J. Ying,[16] S. Yokkaichi,[43,44] G. R. Young,[39] I. Younus,[37] I. E. Yushmanov,[27] W. A. Zajc,[9,†] O. Zaudtke,[34] C. Zhang,[9,39] S. Zhou,[6] J. Zimányi,[25,*] and L. Zolin[22]

(PHENIX Collaboration)

[1]*Abilene Christian University, Abilene, Texas 79699, USA*
[2]*Department of Physics, Banaras Hindu University, Varanasi 221005, India*
[3]*Brookhaven National Laboratory, Upton, New York 11973-5000, USA*
[4]*University of California–Riverside, Riverside, California 92521, USA*
[5]*Charles University, Ovocný trh 5, Praha 1, 116 36 Prague, Czech Republic*
[6]*China Institute of Atomic Energy (CIAE), Beijing, People's Republic of China*
[7]*Center for Nuclear Study, Graduate School of Science, University of Tokyo, 7-3-1 Hongo, Bunkyo, Tokyo 113-0033, Japan*
[8]*University of Colorado, Boulder, Colorado 80309, USA*
[9]*Columbia University, New York, New York 10027, USA, and Nevis Laboratories, Irvington, New York 10533, USA*
[10]*Czech Technical University, Zikova 4, 166 36 Prague 6, Czech Republic*
[11]*Dapnia, CEA Saclay, F-91191 Gif-sur-Yvette, France*
[12]*Debrecen University, H-4010 Debrecen, Egyetem tér 1, Hungary*
[13]*ELTE, Eötvös Loránd University, H - 1117 Budapest, Pázmány P. s. 1/A, Hungary*
[14]*Florida Institute of Technology, Melbourne, Florida 32901, USA*
[15]*Florida State University, Tallahassee, Florida 32306, USA*
[16]*Georgia State University, Atlanta, Georgia 30303, USA*
[17]*Hiroshima University, Kagamiyama, Higashi-Hiroshima 739-8526, Japan*
[18]*IHEP Protvino, State Research Center of Russian Federation, Institute for High Energy Physics, Protvino 142281, Russia*
[19]*University of Illinois at Urbana-Champaign, Urbana, Illinois 61801, USA*
[20]*Institute of Physics, Academy of Sciences of the Czech Republic, Na Slovance 2, 182 21 Prague 8, Czech Republic*
[21]*Iowa State University, Ames, Iowa 50011, USA*
[22]*Joint Institute for Nuclear Research, 141980 Dubna, Moscow Region, Russia*
[23]*KAERI, Cyclotron Application Laboratory, Seoul, South Korea*
[24]*KEK, High Energy Accelerator Research Organization, Tsukuba, Ibaraki 305-0801, Japan*
[25]*KFKI Research Institute for Particle and Nuclear Physics of the Hungarian Academy of Sciences (MTA KFKI RMKI), H-1525 Budapest 114, P.O. Box 49, Budapest, Hungary*
[26]*Korea University, Seoul 136-701, Korea*
[27]*Russian Research Center "Kurchatov Institute," Moscow, Russia*
[28]*Kyoto University, Kyoto 606-8502, Japan*
[29]*Laboratoire Leprince-Ringuet, Ecole Polytechnique, CNRS-IN2P3, Route de Saclay, F-91128 Palaiseau, France*
[30]*Lawrence Livermore National Laboratory, Livermore, California 94550, USA*
[31]*Los Alamos National Laboratory, Los Alamos, New Mexico 87545, USA*
[32]*LPC, Université Blaise Pascal, CNRS-IN2P3, Clermont-Fd, 63177 Aubiere Cedex, France*
[33]*Department of Physics, Lund University, Box 118, SE-221 00 Lund, Sweden*
[34]*Institut für Kernphysik, University of Muenster, D-48149 Muenster, Germany*
[35]*Myongji University, Yongin, Kyonggido 449-728, Korea*
[36]*Nagasaki Institute of Applied Science, Nagasaki-shi, Nagasaki 851-0193, Japan*
[37]*University of New Mexico, Albuquerque, New Mexico 87131, USA*
[38]*New Mexico State University, Las Cruces, New Mexico 88003, USA*
[39]*Oak Ridge National Laboratory, Oak Ridge, Tennessee 37831, USA*
[40]*IPN-Orsay, Universite Paris Sud, CNRS-IN2P3, BP 1, F-91406 Orsay, France*
[41]*Peking University, Beijing, People's Republic of China*
[42]*PNPI, Petersburg Nuclear Physics Institute, Gatchina, Leningrad region, 188300, Russia*
[43]*RIKEN, The Institute of Physical and Chemical Research, Wako, Saitama 351-0198, Japan*
[44]*RIKEN BNL Research Center, Brookhaven National Laboratory, Upton, New York 11973-5000, USA*
[45]*Physics Department, Rikkyo University, 3-34-1 Nishi-Ikebukuro, Toshima, Tokyo 171-8501, Japan*
[46]*Saint Petersburg State Polytechnic University, St. Petersburg, Russia*
[47]*Universidade de São Paulo, Instituto de Física, Caixa Postal 66318, São Paulo CEP05315-970, Brazil*
[48]*System Electronics Laboratory, Seoul National University, Seoul, South Korea*

[49]Chemistry Department, Stony Brook University, Stony Brook, SUNY, New York 11794-3400, USA
[50]Department of Physics and Astronomy, Stony Brook University, SUNY, Stony Brook, New York 11794, USA
[51]SUBATECH (Ecole des Mines de Nantes, CNRS-IN2P3, Université de Nantes) BP 20722, 44307 Nantes, France
[52]University of Tennessee, Knoxville, Tennessee 37996, USA
[53]Department of Physics, Tokyo Institute of Technology, Oh-okayama, Meguro, Tokyo 152-8551, Japan
[54]Institute of Physics, University of Tsukuba, Tsukuba, Ibaraki 305, Japan
[55]Vanderbilt University, Nashville, Tennessee 37235, USA
[56]Waseda University, Advanced Research Institute for Science and Engineering, 17 Kikui-cho, Shinjuku-ku, Tokyo 162-0044, Japan
[57]Weizmann Institute, Rehovot 76100, Israel
[58]Yonsei University, IPAP, Seoul 120-749, Korea

(Received 12 November 2006; published 4 June 2007; corrected 7 June 2007)

The PHENIX experiment at the BNL Relativistic Heavy Ion Collider (RHIC) has measured J/ψ production for rapidities $-2.2 < y < 2.2$ in Au + Au collisions at $\sqrt{s_{NN}} = 200$ GeV. The J/ψ invariant yield and nuclear modification factor R_{AA} as a function of centrality, transverse momentum, and rapidity are reported. A suppression of J/ψ relative to binary collision scaling of proton-proton reaction yields is observed. Models which describe the lower energy J/ψ data at the CERN Super Proton Synchrotron invoking only J/ψ destruction based on the local medium density predict a significantly larger suppression at RHIC and more suppression at midrapidity than at forward rapidity. Both trends are contradicted by our data.

DOI: 10.1103/PhysRevLett.98.232301 PACS numbers: 25.75.Dw

The quark-gluon plasma (QGP) is a state of deconfined quarks and gluons which is predicted by lattice quantum chromodynamics (QCD) calculations to be formed above a temperature T_c of the order of 175–192 MeV for a baryon chemical potential $\mu_b = 0$ [1,2]. Heavy quarkonia (J/ψ, ψ', χ_c, and Υ) have long been considered a promising probe to study the formation and properties of the QGP. In the deconfined state, the attraction between heavy quarks and antiquarks is predicted to be reduced due to dynamic screening effects, leading to the suppression of heavy quarkonia yield. The strength of the suppression depends on the binding energies of the quarkonia and the temperature of the surrounding system [3]. Recent lattice QCD calculations suggest that the J/ψ may not dissociate until well above T_c [4–6]. On the other hand, χ_c and ψ', which contribute to the total J/ψ yield via decay, are expected to dissolve at lower temperatures due to smaller binding energies.

A J/ψ suppression was observed at lower energies by the NA50 experiment at the CERN Super Proton Synchrotron (SPS) [7,8] that could be reproduced by various theoretical calculations [9–13]. Models that invoke the formation of a QGP predict a larger suppression at the BNL Relativistic Heavy Ion Collider (RHIC) than SPS due to the larger energy density of the medium created. On the other hand, several models also predict that the J/ψ yield will result from a balance between destruction due to thermal gluons and enhancement due to coalescence of uncorrelated $c\bar{c}$ pairs [9,14], which are produced abundantly at RHIC energy [15,16]. Cold nuclear matter (CNM) effects such as nuclear absorption, shadowing, and antishadowing are also expected to modify the J/ψ yield. PHENIX d + Au data show that CNM effects are smaller at RHIC than those observed at a lower energy [17] and can be reproduced by a nuclear absorption cross section of up to 3 mb plus nuclear shadowing [18].

We report results on J/ψ production measured by the PHENIX Collaboration at midrapidity ($|y| < 0.35$) via e^+e^- decay and at forward rapidity ($|y| \in [1.2, 2.2]$) via $\mu^+\mu^-$ decay in Au + Au collisions at $\sqrt{s_{NN}} = 200$ GeV. These results do not separate primordial J/ψ and J/ψ from χ_c, ψ', or B decay. The J/ψ invariant yields as a function of centrality, rapidity (y), and transverse momentum (p_T) are shown. They are combined with the yield measured in $p + p$ collisions [19] to form the J/ψ nuclear modification factor R_{AA}.

The PHENIX apparatus is described in Ref. [20]. At midrapidity, electrons are measured with two spectrometers consisting of drift chambers (DC), pad chambers (PC), ring-imaging Cerenkov counters (RICH), and electromagnetic calorimeters (EMCal). They are identified by matching tracks reconstructed with the DC and PC to EMCal clusters and RICH hits. The energy-momentum matching requirement is $(E/p - 1) \geq -2.5$ standard deviations (σ). The position matching between the track and the EMCAL cluster is $\leq 2.5\sigma$ (4σ) in azimuth and along the beam axis, for central (peripheral) collisions. For the RICH, at least 4 (2) matching hits are required. Muons are measured with two spectrometers consisting of a front absorber to stop most hadrons produced in the collision, cathode strip chambers (MuTr), which provide momentum information, and a muon identifier (MuID), which uses alternating layers of steel absorber and Iarocci tubes. Charged particle trajectories are first reconstructed in the MuID and then in the MuTr. They must reach the last plane of the MuID and have a good geometrical match between the MuID and the MuTr to be identified as muons. The matching is $<9°$ for the slope and <15 (20) cm for the position in the first layer of the MuID at positive (negative) rapidity.

The data used for this analysis were collected during the 2004 run at RHIC using a minimum bias trigger (a coincidence of the two beam-beam counters), which covers

$92 \pm 3\%$ of the Au + Au inelastic cross section. After quality assurance and vertex cut ($|z| \leq 30$ cm), 9.9×10^8 (1.1×10^9) events were analyzed for mid (forward) rapidity, corresponding to an integrated luminosity of 157 μb^{-1} (174 μb^{-1}).

The J/ψ yield is obtained from the unlike-sign dilepton invariant mass distribution [21] after subtracting the combinatorial background using an event-mixing technique. The background is normalized to the real data by equating $2\sqrt{N^{++}N^{--}}$, with N^{++} (N^{--}) being the number of positive (negative) dilepton pairs. The accuracy of the normalization is estimated to be 2% and is accounted for in the systematic errors. At midrapidity, the J/ψ mass resolution is ~ 35 MeV/c^2. The number of J/ψ is determined by counting the remaining unlike-sign pairs in the mass range $2.9 \leq M \leq 3.3$ GeV/c^2. This number is corrected by the estimated contribution of the dielectron continuum and the loss due to the radiative tail. A total of $\sim 1000 J/\psi$ are obtained, and the signal to background (S/B) varies from 0.5 for central collisions to 15 for peripheral collisions. At forward rapidity, the J/ψ mass resolution varies from 150 to 200 MeV/c^2 and is larger than at midrapidity primarily because of the multiple scattering and energy loss straggling in the front absorber. The residual background (notably, open charm pairs and Drell-Yan processes) in the unlike-sign invariant mass distribution is evaluated using an exponential form. The J/ψ signal is estimated by counting the remaining pairs in the mass range $2.6 \leq M \leq 3.6$ GeV/c^2 and using a fit with different line shapes. The average of the resulting values is used as the number of J/ψ, and their dispersion is included in the systematic error. A total of $\sim 4500 J/\psi$ are obtained, and S/B varies from 0.2 for central collisions to 3 for peripheral collisions.

The J/ψ invariant yield in a given centrality, p_T, and y bin is

$$\frac{B_{ll}}{2\pi p_T}\frac{d^2N_{J/\psi}}{dp_T dy} = \frac{1}{2\pi p_T}\frac{N_{J/\psi}}{N_{\mathrm{evt}}\Delta y \Delta p_T A\varepsilon}, \qquad (1)$$

with B_{ll} being the branching ratio for $J/\psi \to l^+l^-$, $N_{J/\psi}$ the number of J/ψ measured in the bin, N_{evt} the corresponding number of events, and $A\varepsilon$ the acceptance and efficiency correction for J/ψ. $A\epsilon$ is determined by full GEANT simulation. It decreases with the collision centrality due to overlapping hits in the RICH, EMCal, and MuTr, leading to an increasing number of misreconstructed tracks, which are then rejected by the analysis cuts. This effect is evaluated by embedding simulated J/ψ in real events. For the most central collisions, the efficiency loss is 20% at midrapidity and 75% (50%) at positive (negative) rapidity.

The nuclear modification factor in a given centrality, p_T, and y bin is

$$R_{AA} = \frac{d^2N^{AA}_{J/\psi}/dp_T dy}{N_{\mathrm{coll}} d^2N^{pp}_{J/\psi}/dp_T dy}, \qquad (2)$$

TABLE I. Sources of systematic errors on the J/ψ invariant yield. When two values are given, the first (second) is for peripheral (central) collisions. Errors of type A (type B) are point-to-point uncorrelated (correlated).

Source	$\|y\| < 0.35$	$\|y\| \in [1.2, 2.2]$	Type
Signal extraction	6.5%–9%	4%–24%	A
Acceptance	6%	10%	B
Efficiency	4.5%–8%	4%–16%	B
Run by run variation	4%	5%	B
Input y, p_T distributions	2%	4%	B

with $d^2N^{AA}_{J/\psi}/dp_T dy$ being the J/ψ yield in Au + Au collisions, N_{coll} the mean number of binary collisions in the centrality bin, and $d^2N^{pp}_{J/\psi}/dp_T dy$ the J/ψ yield in $p + p$ inelastic collisions.

The systematic errors on the J/ψ invariant yield (Table I) are grouped into three categories: point-to-point uncorrelated (type A), for which the points can move independently one from the other; point-to-point correlated (type B), for which the points can move coherently, though not necessarily by the same amount; and global errors, for which all points move by the same relative amount. Statistical and type A errors are summed in quadrature and represented with vertical bars; type B errors are represented with boxes, and different colors or symbols are used for forward and midrapidity because they are independent; global systematic errors are quoted in the figures. For R_{AA}, additional errors are associated with uncertainties in the calculation of N_{coll} (10%–28%) and the J/ψ yield in $p + p$ (12% and 7% at mid and forward rapidity, respec-

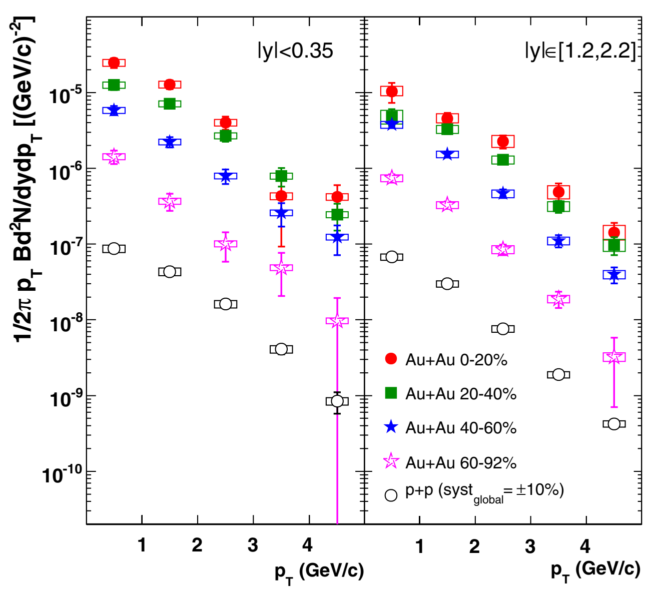

FIG. 1 (color online). J/ψ invariant yield versus p_T for different centrality bins in Au + Au collisions and in $p + p$ collisions [19]. The left (right) panel corresponds to mid (forward) rapidity. See text for description of the errors and Ref. [21] for data tables.

TABLE II. Characterization of the J/ψ, p_T, and y distributions. Column 3 (4): J/ψ $\langle p_T^2 \rangle$ calculated for $p_T \leq 5$ GeV/c at mid (forward) rapidity for different centrality bins in Au + Au collisions and in $p + p$ collisions. The first error corresponds to statistical and type A. The second error is type B.

Percent (%)	N_{part}	$\langle p_T^2 \rangle$ (GeV/c)^2 $\lvert y \rvert < 0.35$	$\langle p_T^2 \rangle$ (GeV/c)^2 $1.2 < \lvert y \rvert < 2.2$	y rms
0–20	280	3.6 ± 0.6 ± 0.1	4.4 ± 0.4 ± 0.4	1.32 ± 0.06
20–40	140	4.6 ± 0.5 ± 0.1	4.6 ± 0.3 ± 0.4	1.30 ± 0.05
40–60	60	4.5 ± 0.7 ± 0.2	3.7 ± 0.2 ± 0.3	1.40 ± 0.04
60–92	14	3.6 ± 0.9 ± 0.2	3.3 ± 0.3 ± 0.2	1.43 ± 0.04
$p + p$	2	4.1 ± 0.2 ± 0.1	3.4 ± 0.1 ± 0.1	1.41 ± 0.03

tively). On the other hand, some errors that are common to Au + Au and $p + p$ cancel.

Figure 1 shows the J/ψ yield versus p_T for different centrality bins (see Table II for the corresponding number of participants N_{part}). Data from the two muon spectrometers are combined to obtain the forward rapidity points. In each centrality bin, the J/ψ mean square transverse momentum $\langle p_T^2 \rangle$ is numerically calculated for $p_T \leq 5$ GeV/c and is shown in Table II. At midrapidity, the $\langle p_T^2 \rangle$ shows no variation versus centrality within errors. It increases slightly with N_{part} at forward rapidity.

Figure 2 shows the J/ψ yield versus y for different centrality bins. The root mean square (rms) of each distribution is shown in Table II. For the two most peripheral bins, the rms is compatible with that measured in $p + p$ collisions. For the most central bins, the rms is smaller by about 2σ.

Figures 3 and 4 show the J/ψ R_{AA} versus p_T and y, respectively, for different centrality bins. Figure 5(a) shows the p_T integrated R_{AA} versus N_{part} at mid and forward rapidity, respectively. For each rapidity, R_{AA} decreases with increasing N_{part}. For the most central collisions, R_{AA} is below 0.3 (0.2) at mid (forward) rapidity. Figure 5(b) shows the ratio of forward or midrapidity R_{AA} versus N_{part}. The ratio first decreases and then reaches a plateau of about 0.6 for $N_{part} > 100$.

In summary, a significant J/ψ suppression relative to the binary scaling of proton-proton collisions is observed for central Au + Au collisions at RHIC. Its magnitude is greater than that expected by extrapolating the CNM effects measured in d + Au collisions [17,18,22]. At midrapidity, the suppression is similar to that observed at the SPS [8], whereas at forward rapidity it is significantly larger. Models of quarkonia suppression driven by the local energy density of the medium predict a greater suppression at RHIC than SPS and less suppression at forward rapidity than at midrapidity [9,10]. Both trends are contradicted by

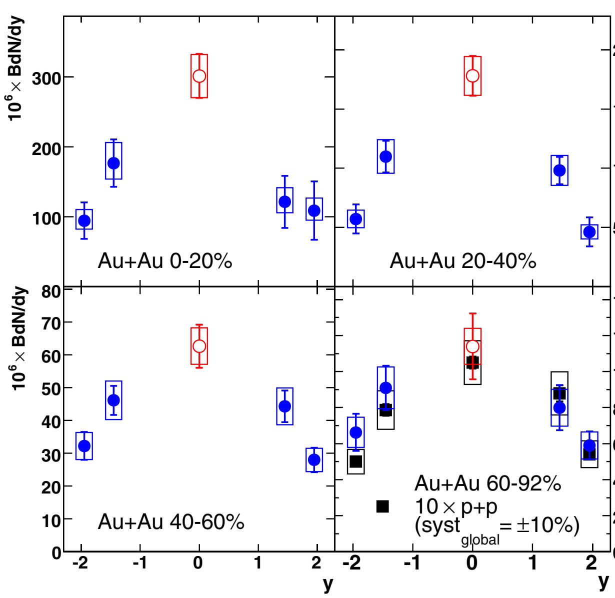

FIG. 2 (color online). J/ψ invariant yield versus y for different centrality bins in Au + Au collisions and for $p + p$ collisions. Open (solid) circles are for mid (forward) rapidity Au + Au data. Black squares are for $p + p$ data [19]. See text for description of the errors and Ref. [21] for data tables.

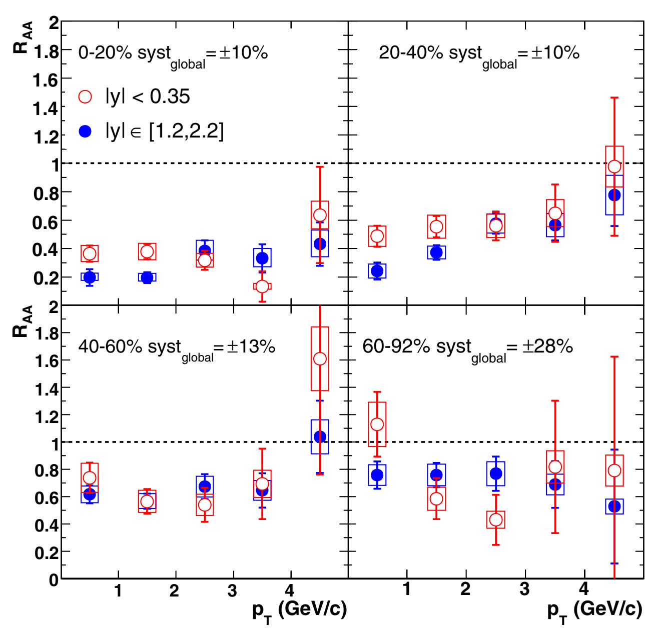

FIG. 3 (color online). J/ψ R_{AA} versus p_T for several centrality bins in Au + Au collisions. Mid (forward) rapidity data are shown with open (solid) circles. See text for description of the errors and Ref. [21] for data tables.

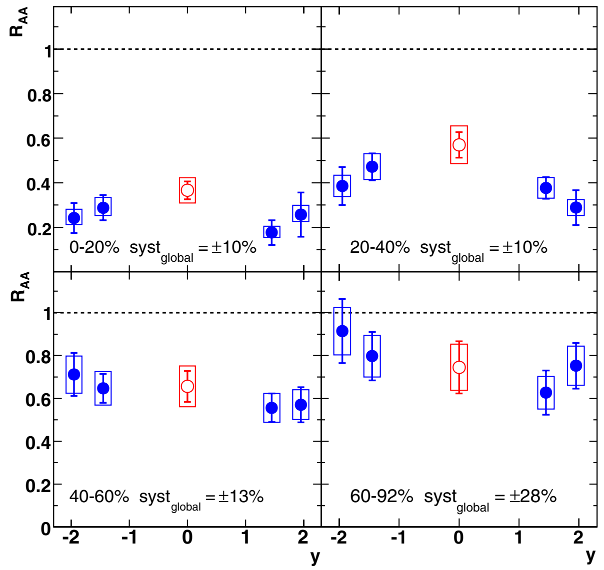

FIG. 4 (color online). J/ψ R_{AA} versus y for different centrality bins. Open (solid) circles are for mid (forward) rapidity. See text for description of the errors and Ref. [21] for data tables.

our data. Additionally, the J/ψ mean square transverse momentum, restricted to $p_T \leq 5$ GeV/c, shows little dependence on centrality. Various models of J/ψ production and suppression, which predict different transverse momentum and rapidity dependencies, can be significantly constrained by the data presented here and recent results on the open charm [16].

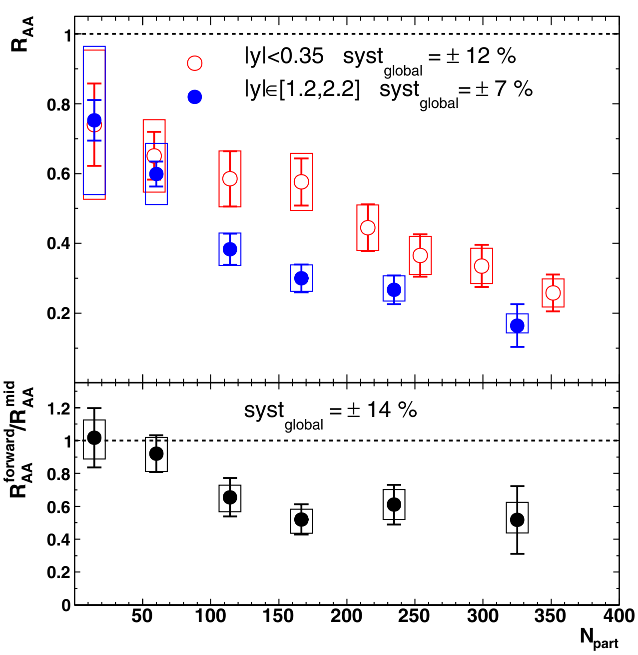

FIG. 5 (color online). (a) J/ψ R_{AA} versus N_{part} for Au + Au collisions. Mid (forward) rapidity data are shown with open (solid) circles. (b) Ratio of forward or midrapidity J/ψ R_{AA} versus N_{part}. For the two most central bins, midrapidity points have been combined to form the ratio with the forward rapidity points. See text for description of the errors and Ref. [21] for data tables.

We thank the staff of the Collider-Accelerator and Physics Departments at BNL for their vital contributions. We acknowledge support from the Office of NP in DOE Office of Science and NSF (USA), MEXT and JSPS (Japan), CNPq and FAPESP (Brazil), NSFC (China), MSMT (Czech Republic), IN2P3/CNRS and CEA (France), BMBF, DAAD, and AvH (Germany), OTKA (Hungary), DAE (India), ISF (Israel), KRF and KOSEF (Korea), MES, RAS, and FAAE (Russia), VR and KAW (Sweden), U.S. CRDF for the FSU, U.S.–Hungarian NSF-OTKA-MTA, and U.S.–Israel BSF.

*Deceased.
†PHENIX Spokesperson.
Electronic address: zajc@nevis.columbia.edu

[1] Y. Aoki, Z. Fodor, S. D. Katz, and K. K. Szabo, Phys. Lett. B **643**, 46 (2006).
[2] M. Cheng *et al.*, Phys. Rev. D **74**, 054507 (2006).
[3] T. Matsui and H. Satz, Phys. Lett. B **178**, 416 (1986).
[4] S. Datta, F. Karsch, P. Petreczky, and I. Wetzorke, Phys. Rev. D **69**, 094507 (2004).
[5] M. Asakawa and T. Hatsuda, Phys. Rev. Lett. **92**, 012001 (2004).
[6] T. Umeda, K. Nomura, and H. Matsufuru, Eur. Phys. J. C **39S1**, 9 (2005).
[7] M. C. Abreu *et al.*, Phys. Lett. B **410**, 337 (1997).
[8] B. Alessandro *et al.*, Eur. Phys. J. C **39**, 335 (2005).
[9] L. Grandchamp, R. Rapp, and G. E. Brown, Phys. Rev. Lett. **92**, 212301 (2004).
[10] A. Capella and E. G. Ferreiro, Eur. Phys. J. C **42**, 419 (2005).
[11] X.-l. Zhu, P.-f. Zhuang, and N. Xu, Phys. Lett. B **607**, 107 (2005).
[12] E. L. Bratkovskaya, A. P. Kostyuk, W. Cassing, and H. Stocker, Phys. Rev. C **69**, 054903 (2004).
[13] A. Andronic, P. Braun-Munzinger, K. Redlich, and J. Stachel, Phys. Lett. B **571**, 36 (2003).
[14] R. L. Thews and M. L. Mangano, Phys. Rev. C **73**, 014904 (2006).
[15] S. S. Adler *et al.*, Phys. Rev. Lett. **96**, 032301 (2006).
[16] A. Adare *et al.*, Phys. Rev. Lett. **97**, 252002 (2006).
[17] S. S. Adler *et al.*, Phys. Rev. Lett. **96**, 012304 (2006).
[18] R. Vogt, Acta Phys. Hung. **A25**, 97 (2006).
[19] A. Adare *et al.*, preceding Letter, Phys. Rev. Lett. **98**, 232002 (2007).
[20] K. Adcox *et al.*, Nucl. Instrum. Methods Phys. Res., Sect. A **499**, 469 (2003).
[21] See EPAPS Document No. E-PRLTAO-98-009723 for plain text data files for all of the plotted data points, plots from the figures but with the PHENIX logo for presentations, and mass spectra plots. For more information on EPAPS, see http://www.aip.org/pubservs/epaps.html.
[22] R. Granier de Cassagnac, arXiv:hep-ph/0701222.